Measurement of Creep Deformation across Welds in 316H Stainless Steel Using Digital Image Correlation

Journal Item

oro.open.ac.uk

CrossMark

Measurement of Creep Deformation across Welds in 316H Stainless Steel Using Digital Image Correlation

Y. Sakanashi[1] · S. Gungor[1] · A.N. Forsey[1] · P.J. Bouchard[1]

Abstract Spatially resolved measurement of creep deformation across weldments at high temperature cannot be achieved using standard extensometry approaches. In this investigation, a Digital Image Correlation (DIC) based system has been developed for long-term high-temperature creep strain measurement in order to characterise the material deformation behaviour of separate regions of a multi-pass weld. The optical system was sufficiently stable to allow a sequence of photographs to be taken suitable for DIC analysis of creep specimens tested at a temperature of 545 °C for over 2000 h. The images were analysed to produce local creep deformation curves from two cross-weld samples cut from contrasting regions of a multi-pass V-groove weld joining thick-section AISI Type 316H austenitic stainless steel. It is shown that for this weld, the root pass is the weakest region of the structure in creep, most likely due to the large number of thermal cycles it has experienced during the fabrication process. The DIC based measurement method offers improved spatial resolution over conventional methods and greatly reduces the amount of material required for creep characterisation of weldments.

✉ A.N . Forsey
alex.forsey@open.ac.uk

[1] Materials Engineering, School of Engineering and Innovation, The Open University, Walton Hall, Milton Keynes MK7 6AA, UK

Introduction

Pressure vessel and piping systems operating at high temperature, where material may deform in a time dependent manner, are vulnerable to creep damage accumulation leading to cavity nucleation and growth around welded regions. This degradation mechanism can reduce component lifetime and challenge the structural integrity of welded joints and critical systems (for example [1]). Creep deformation and damage mechanisms driving failure of weldments are not well understood owing to the variation in composition, microstructure, properties and constraint across a typical joint, as well as the influence of geometry, residual stress, elastic follow-up, primary load, the effect of cyclic loading and environment. Creep life assessment of power plant systems [2] requires knowledge of the local creep properties of components at the most vulnerable locations, for example the heat affected zone (HAZ), or weld metal, of welded joints.

The traditional method for measuring the variation in creep deformation and rupture properties across a weldment is to cut small specimens from the weld, the HAZ (a region of the parent material where the microstructure has been altered by the heat from the welding process) and the parent material. Individual uniaxial creep tests are then carried out, in which the average strain response of the test sample gauge length with time is measured using standard extensometry [3]. Such tests usually give properties aligned with the direction of welding (referred to as the longitudinal direction) and a macroscopic measure of the creep properties averaged across several millimetres (dependent on the cross-section dimensions of the test specimen). This type of materials properties test programme consumes a large volume of weldment material (which may be scarce) and it may not even be feasible to extract test samples, of a practical size, from the required locations. It is then often assumed that the creep properties

measured in the weld longitudinal direction apply in the transverse directions (i.e. the material constituents of the welded joint exhibit isotropic behaviour). Conventional creep life assessment methods use uniaxial material properties that reflect the local material behaviour, which is dependent on the microstructure and thermo-mechanical history. The assessment method, whether code, standard or FEA, then accounts for geometry, mismatch, constraint, residual stress, load, and elastic follow up. The aim of using DIC strain measurement during creep tests is to get local creep properties to go into these assessment methods, for which we must avoid geometry, mismatch and constraint effects.

This paper presents an experimental technique for measuring the creep deformation response at millimetre length-scale spanning a "cross-weld" specimen during creep rupture testing. The creep properties measured in a direction transverse to the weld line are more relevant to component life assessment than those measured parallel to the welding direction. It is not possible to measure transverse weldment creep properties at millimetre length scales using traditional approaches. Spatially resolved measurement of room temperature tensile properties in cross-weld samples has been applied in several laboratories using DIC [3–8]. This method involves testing a tensile specimen containing the main part of the weldment within its gauge length, and mapping the full deformation field along the gauge section through computational tracking of contrasting surface features (speckle patterns) on a sequence of digital images of the specimen's gauge section taken during the test.

Recently the present authors have demonstrated the use of a DIC technique for the measurement of strain during uniaxial tensile and time-dependent creep rupture tests at elevated temperatures [9, 10]. The present article describes in detail the test set-up for the DIC measurements and the analysis methods developed to measure spatially resolved creep deformation properties in cross-weld samples extracted from multi-pass weldments. This is believed to be the first example of a DIC monitored creep test across a weldment reported in the literature.

Experimental

Materials

The weldment studied in this work is a specially designed thick section austenitic stainless steel (AISI Type 316H) multi-pass weldment supplied by EDF Energy. It was made from an ex-service AISI Type 316H austenitic stainless steel pressure vessel of outer diameter 430 mm and 64 mm wall thickness. The completed weldment is illustrated in Fig. 1, and shows extraction locations for the cross-weld creep test specimens described later. The weld preparation is unusual being

asymmetric, with one sidewall perpendicular to the inner/outer surfaces. This geometry was designed to give a fusion boundary suitable for extraction of compact tension specimens for creep crack growth tests close to the weld/HAZ fusion interface. This weldment configuration also facilitated extraction of cross-weld samples for the present tests and other programs. The parent material to the right of the vertical weld preparation came from header HYA 2D2/2 (cast 55,882 with 0.08% N content), which had been in service for 65,000 h at a mean equivalent creep temperature of 519 °C (and would have been in a solution heat treated state at time of installation). Parent material adjacent to the inclined weld prep came from header HYA 1D2/4 (cast 53,547 with 0.029% N content), which had been in service for 87,000 h at a mean equivalent creep temperature of 515 °C. A circumferential gas tungsten arc welding (GTAW) process was applied for the root run (the first pass) using a 2.4 mm diameter tungsten inert gas (TIG) wire. A shielded metal arc welding (SMAW) process was used with 3.2 mm diameter Babcock S electrodes (AWS A5.4 E316L-15) for the 129 fill passes deposited in 26 layers starting at the root. This cylindrical butt weld was made by EDF Energy from scarce parent material, cut from ex-service pressure vessels for testing the creep behaviour of new weldments made from service aged material. This combination of materials was of interest because when operating components are replaced or repaired, new welds are introduced which can adversely influence the state of in-situ service aged material.

High Temperature DIC System for Creep Tests

Digital Image Correlation

The DIC software used in these investigations is DaVis 8.2 [11] provided by LaVision GmbH. The correlation method uses the sum of square differences (SSD) [12] method, which is solved iteratively via least-squares. For each image the algorithm initially calculates the displacement of a single point (seed point) via the Lucas-Kanade method [13] using the implementation of Bouguet [14]. This uses a pyramidal approach to allow for large displacements between images by binning pixels to allow a search over a larger area. Once the displacement of the seed point is calculated for each image, the result is used as the initial condition for the second part of the algorithm as part of the "region grow" approach.

Affine transforms are included in the SSD function to permit first order sub-region deformation of the reference image [15]. This allows the accommodation of strains and rotations of the deformed image. To improve the preservation of the phase component in the interpolated sub-pixel displacement grey level values, the interpolation is carried out using spline-6 interpolation, rather than bilinear for the calculation of the displacement of the seed point.
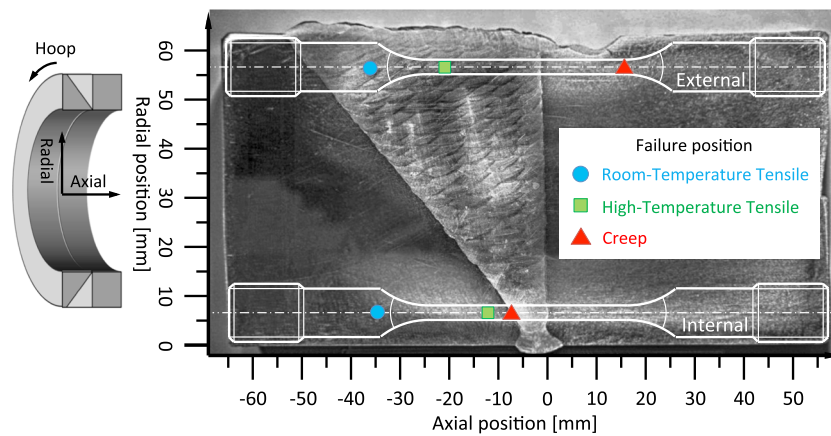
Fig. 1 Thick section (64 mm) austenitic stainless steel weldment showing creep test specimen extraction locations. Specimen rupture positions in cross-weld tensile tests and creep tests are also shown (note the room temperature specimens used a longer gauge length of 70 mm). Schematic diagram inset shows the orientation of the weld in the pipe section

Lyons et al. [16] were the first to demonstrate that DIC monitoring could be applied to measure surface deformation and strain at high temperatures, measuring free thermal expansion and strains due to tensile loads in Inconel 718 superalloy specimens at temperatures up to 650 °C. They identified measurement errors caused by image distortion due to (i) imperfections in the furnace window and (ii) variations in refractive index of heated air between the furnace window and the camera lens. They managed to reduce the errors by using an optical quality furnace window and introducing turbulent mixing of the air outside of the furnace by using a fan.

Colour cameras were used for obtaining the images for the long-term DIC experiments presented in this manuscript. This is not considered good practice, but for long term testing, these consumer products possess a number of advantages over a scientific camera. The principal advantages for using these cameras are long-term reliability, low cost and high-resolution imaging. Many of the disadvantages that are associated with using consumer cameras for DIC are also less of a concern for long term testing. Sensor temperature increase during repeated imaging leading to increased dark current noise does not occur during a creep test. This is because the imaging is so infrequent that there is little opportunity for the sensor temperature to vary in a lab with tightly controlled air conditioning, despite the lack of active cooling. During a creep test there is little time pressure to take each image, so any vibration due to shutter movement can be allowed to dissipate before the image is acquired. The mosaic image created by the colour filter array can be converted into greyscale suitable for DIC that does not produce significant integer bias, thus high resolution images can be obtained from these cameras for use with DIC [17]. This camera system was suboptimal for the validation tensile test described in Validation of DIC Monitoring System section, due to the rapid imaging requirements of such a test, but was used to enable transferability of findings.

Experimental Set-Up for Creep and High Temperature Tensile Testing

Two types of test were conducted: long-term load controlled high temperature creep deformation/rupture tests and high temperature tensile tests. Figure 2(a) shows the DIC high temperature creep deformation measurement system developed for the present work. A three-zone furnace was specially manufactured with a porthole through its wall for the purpose of imaging the specimen surface during testing. A temperature survey of this furnace and assembly was performed by Sakanashi [18] using 8 thermocouples. It was found that the temperature was essentially uniform (within ±1 °C) along the sample and hence the temperature of the sample's gauge section could be confidently determined by referencing just two thermocouples. In this way the risk of the thermocouples obscuring the images for DIC could be avoided. The furnace was fitted to a standard lever-arm load frame used for creep deformation and rupture. An optical quality sapphire window covering the porthole was fitted to the outside of the creep furnace. The window was sealed using high temperature silicone sealant to prevent escape of heated air, which could affect the light path to the camera and cause image distortion. The 20 mm wide by 40 mm high porthole dimensions were chosen to minimise the potential influence of the access hole on the uniformity of the temperature distribution within the furnace, but this restricted the field of view of the specimen by the camera.

An Instron 8862 slow strain rate tensile testing machine with a 100 kN load cell was used for tensile validation tests. Cooling the pull-rods using recirculating chilled water protected the integrity of the load frame and the load cell. A three-zone furnace was used to heat the test specimens on the testing machine, enabling fine control of temperature along the specimen. This tensile testing furnace had an open porthole 30 mm high by 15 mm wide at mid-height, covered with an optical quartz window for DIC monitoring, in a similar
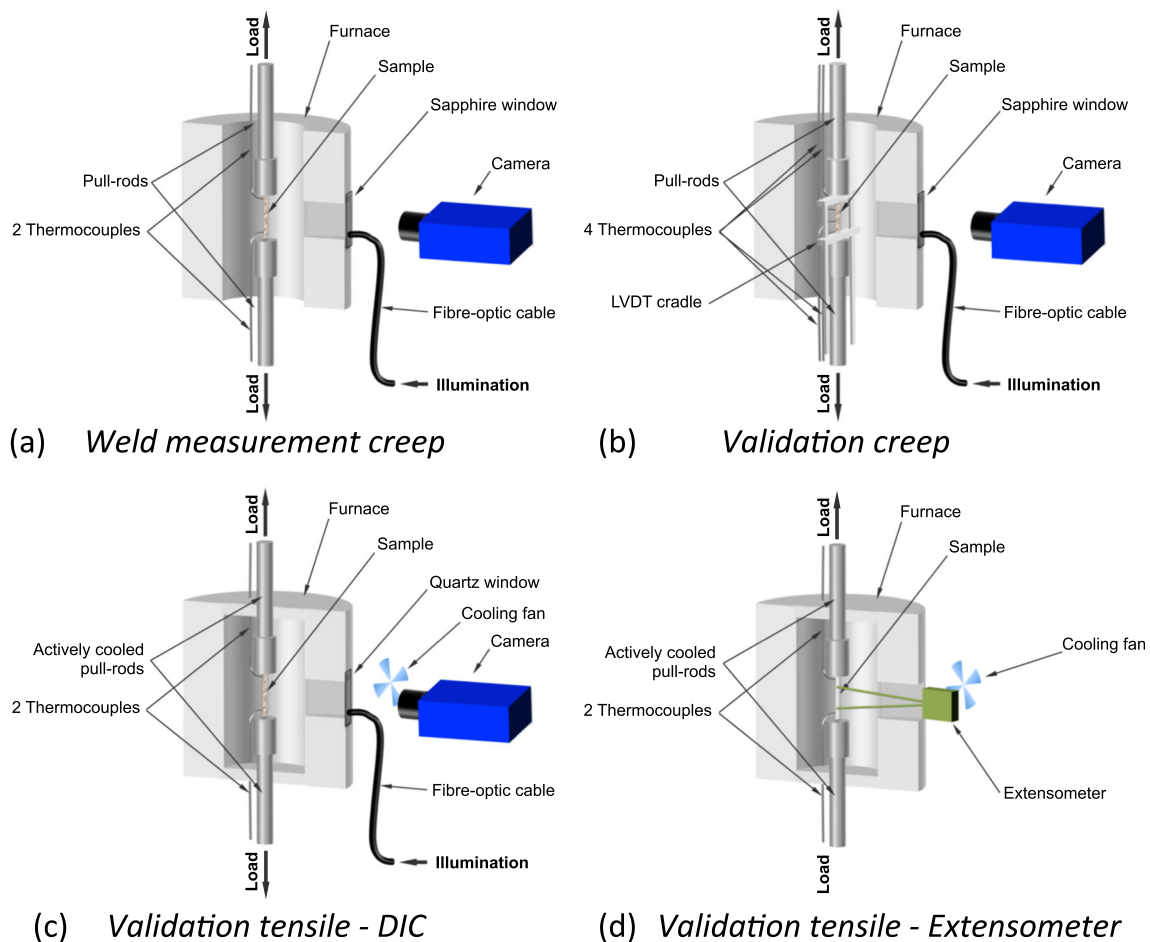
(a) *Weld measurement creep*

(b) *Validation creep*

(c) *Validation tensile - DIC*

(d) *Validation tensile - Extensometer*

Fig. 2 Schematic diagrams showing the main components of the high temperature DIC measurement system used for (**a**) the weld creep tests, (**b**) validation creep tests and (**c**) tensile validation test. The non-DIC set-up using a side-entry extensometer in place of the window is also shown in (**d**)

manner to the sapphire window on the creep furnace mentioned previously. A fan was used to mix the air between the window and the camera lens in order to reduce image distortion due to thermal air currents arising from imperfect sealing of the window. A schematic diagram of the set-up can be seen in Fig. 2(c).

A flat-sided test specimen was designed for the DIC monitored creep tests as shown in Fig. 3. The gauge length has a rectangular cross-section (6 mm width and 3 mm thickness) and blends to standard M12 threaded ends. The blend radius was chosen based upon finite element studies to minimise stress concentration effects. The specimen was fixed into the loading frame using screwed joints inside the furnace, and the tips of two thermocouples were inserted into small drilled holes at the top and bottom of the specimen, beyond the gauge section. The vertical position and rotation of the load string were carefully adjusted to give the digital camera the required view of the gauge section through the window.

A Nikon D300 digital single-lens reflex (DSLR) camera with a resolution of 4288 × 2848 pixels, a 150 mm focal length macro lens (Sigma 150 mm f2.8 APO macro DG HSM), Novoflex Ballpro macro bellows and a 300 mm object working distance were used for the tensile tests and cross-weld creep tests described here. A Nikon D810 DSLR with a resolution of 7360 × 4912 pixels, a 200 mm focal length macro lens (Nikkor 200 mm micro f4 IF-ED), Novoflex Ballpro macro bellows and a 400 mm object working distance were used for the creep validation tests. Images of the specimen surface during testing were acquired at regular intervals using time-lapse photography software (Nikon Camera-Control-Pro). For all tests an aperture of f16 and a flash synch shutter speed of 1/160 s were used. For the high temperature tensile test, a synchronous trigger was used to begin the image recording and the test program. The time base from each PC was then used to match the load data to the images.

The sample surface was illuminated using a fibre optic light bundle, coupled to an external flash unit triggered by the digital camera. Due to a colour camera being used for these experiments, it was not possible to use a coloured filter to block the blackbody radiation (as reported in other high temperature DIC tests [19]), because this would have significantly reduced the effective resolution of the camera. However, the standard Nikon D810 camera does have a near infrared filter, which will reduce some of this effect. In addition, high intensity flash

Fig. 3 Test specimen design developed for use in DIC creep tests
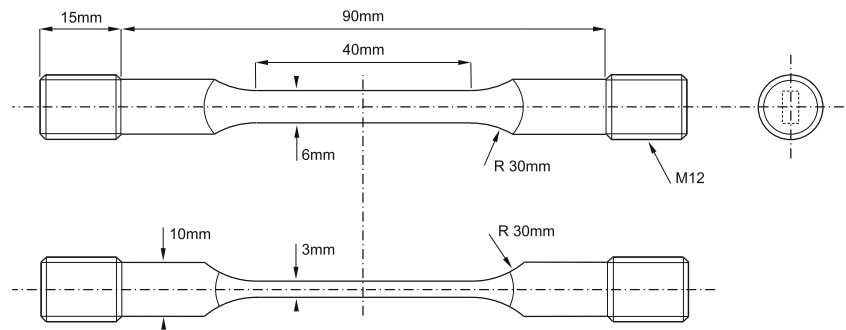
illumination was chosen to illuminate the sample surface, which rendered the additional light from the blackbody radiation to be negligible compared with the measured signal.

The vibration due to mirror retraction in the D300 camera was minimised by using a three second shutter delay. This leaves the shutter as the only moving part required to take the image. This further potential cause of camera vibration was removed through using the D810 camera, with its electronic front curtain shutter feature [20], for the creep validation test. No measureable difference was found between the images captured with the mechanical or electronic shutter features of the D810 camera. This outcome is attributed to the rigid fixing of the D810 camera and the relatively low mass of the shutter mechanism. Although the shutter mechanism of the D300 is of a different construction from that of the D810, it is similarly unlikely to cause a measurable error. The shutter in the D300 is also of a smaller size, due to the smaller size of the sensor, and the physical size of the pixels is larger (5.5 μm for the D300 as opposed to 4.88 μm for the D810), reducing its sensitivity to vibration.

An important consideration for high temperature application of DIC is the stability of the appearance of the test surface during the experiment. The measurement accuracy is principally dependent on the identification of contrasting surface features (i.e. speckles), which can be adversely affected by oxidation. In the present work, specimen surfaces were coated with a silica ceramic-based paint (VHT FlameProof™). This provided a non-degrading appearance for the material tested. The speckle pattern was produced by using paint of two different shades. First, a coat of matte white paint was applied on the gauge length surface of the specimens, to prevent any direct reflections from the sample surface. Second, a matte black spray paint was used to create a random speckle on the white base. After application, the paint was cured at three temperatures (the highest of which was 315 °C), as specified by the supplier. Figure 4 shows a typical speckle pattern obtained on the surface of a stainless steel specimen.

DIC Analysis Procedure

The working principle of DIC is based on optical flow estimation [15], so that grey value (i.e. light intensity) patterns in

digital images of the test surface are tracked across multiple images taken before and after surface deformation [21]. An important parameter in DIC analysis is the speckle size [22, 23]. If the speckle size is too large, the subset size must be increased to achieve accurate correlation, but increasing the subset size reduces the spatial resolution [23]. In this study, the imaging system was set up to give a pixel size of about 10 μm and the corresponding speckle size was approximately 50 μm, which was found to give good correlation in the DIC analysis.

Raw to Greyscale Conversion

The cameras used in this study have a colour filter array [24] applied in a Green-Blue-Red-Green (GBRG) formation. For DIC a greyscale image is required, that is, a light intensity value for each pixel rather than a colour value. Hence, the colour information from the Bayer filter must be converted to a monochrome image. The sections below describe how the recorded images were converted to greyscale and the procedure followed in the calculation of strain maps. The images in this study were recorded in Nikon's 14 bit uncompressed raw format, which contained the intensity information of each pixel. The images were imported into a Matlab [25] script, in which greyscale conversion was performed as described below, so that the monochrome image produced from the raw colour information was optimal for use with DIC [17].

The monochrome conversion begins with the RGB values for every pixel being calculated using interpolation. For the green channel, every pixel point has the average intensity of all the green pixels within one pixel of the position being considered (a region of 3 × 3 pixels), but with a linear fit applied. The process is repeated for both the red and blue channels, but these channels have half the number of sensitive pixels. With the red, green and blue channels calculated for every point, they are summed for each position, giving equal weighting to each of the red and blue channels and double the weighting for the green channel. The green channel has twice the number of photosites per unit area and so has twice the weight. The result was normalised by removing the extreme 0.01% of the intensity values from either end of the range. The

Fig. 4 Photograph of small region of external sample surface after application and curing of paint layers showing the speckle pattern achieved
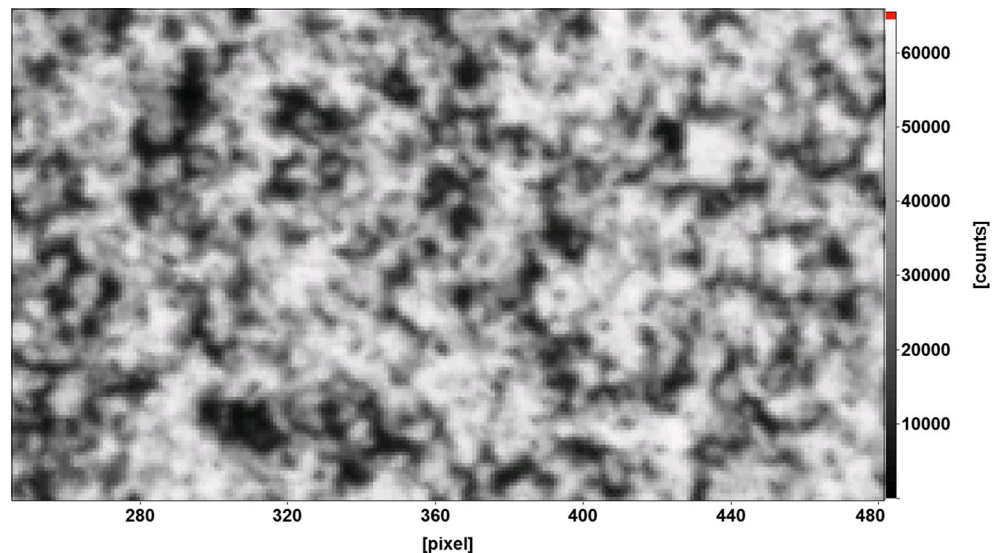

image is then quantised to the full 16 bit range and saved as an uncompressed *tif* file.

Displacement Calculation

Displacement vectors were calculated using the commercial program DaVis 8.2 by LaVision [11]. The correlation calculation used the first image as the reference and was performed using a least squares approach over a 31×31 pixels region with an interval between the centres of each region of 7 pixels. For the creep tests, the first image of the data set was taken immediately after the load was applied, so only creep strain is measured. It was not possible to obtain a satisfactory reference image at zero load due to the lack of sample constraint at zero load associated with the long load chain typically found on a creep frame. This lack of constraint permits the sample to move out of plane and so invalidate the assumption required for 2D DIC that all deformation occurs in-plane. The high temperature tensile test was performed on a standard universal testing machine and so the load chain was more rigid,

Table 1 Algorithm settings used for DIC calculation

Parameter	Value/setting
Pyramid Levels	2
Epsilon	0.01
Correlation threshold	0.2
Threshold confidence margin	0.01
Subregion weighting	Round Gaussian
Sub-pixel interpolation	Bi-cubic spline
Normalisation	At subregion scale

allowing a reference image to be taken at zero load. The remaining correlation settings can be seen in Table 1.

Strain Calculation

When calculating strain from displacement data, a differentiation step is required and the result is very sensitive to noise in the raw data. Therefore, either averaging over a larger region or smoothing the result using a smaller region is required to produce satisfactory strain data. In this work an averaging method was used, and this removed the need for smoothing of either the strain fields or the strain-time curves. Averaging the strain across the width of the sample, in combination with a constant strain assumption, allows the plotting of a strain-time curve at any position along the length of the sample. To achieve this, the output vector fields from the DIC analysis from DaVis 8.2 were sampled to form 100 equal sized rectangular regions along the length, as shown in Fig. 5, using in-house software written in Matlab. These regions were overlapped by 75% to increase spatial resolution and each region sampled a 1 mm length of the sample gauge. 10% of the sample width closest to each edge was excluded from the calculation to prevent spurious vectors caused by the less constrained vectors from the edges of the sample from adversely affecting the results.

A schematic diagram of the strain-processing algorithm can be seen in Fig. 5. This shows a first-order two-dimensional polynomial fitted to the displacement vectors in the x-direction (i.e. across the width of the gauge section) and y-direction (i.e. along the gauge length) separately for each region in each image, using a least-squares approach [26]. The difference between the fit and the measured displacements was used to identify any vectors more than 3 standard deviations from the mean, which were subsequently removed. The fits were
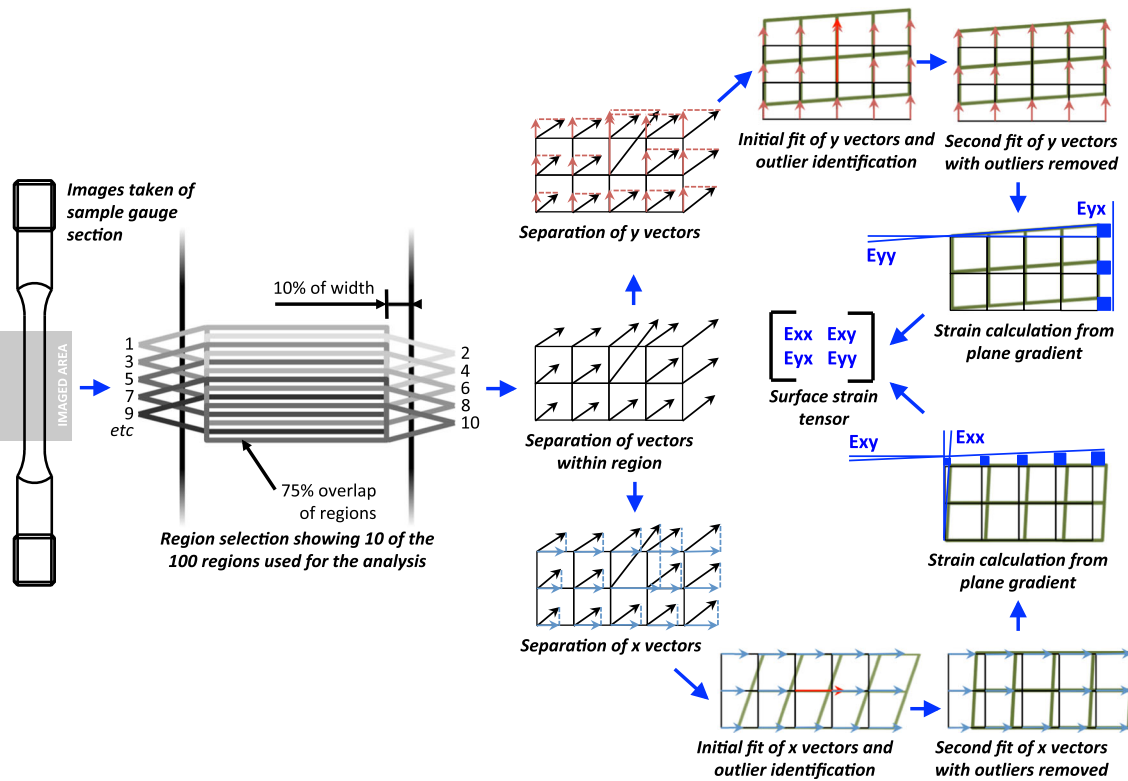
Fig. 5 Schematic diagram showing the spatial strain averaging procedure used to extract high quality creep curves from the DIC displacement data

performed for a second time. The gradients of the two fitted polynomials (*x* and *y* data) were then taken as the differential of the displacements for the whole region for that time-step (image) and converted to Lagrange strain. By assuming constant strain in each region, strain-time curves for 100 equal sized regions of the sample were plotted for the stainless steel specimens.

Validation of DIC Monitoring System

Two high temperature tensile tests were carried out at 550 °C on identical AISI Type 316H stainless steel specimens, but with no weld present. Both tensile tests were carried out using an extension rate of 0.1 mm/min. To verify the accuracy of the DIC measurement technique, on one of the samples the extension of the gauge section was measured using a conventional extensometer (Fig. 2(d)) and the other using DIC (Fig. 2(c)). Two tests were required because the furnace used only has a single opening, which can be used for either imaging or an extensometer. Both tests were continued until the specimens failed. During the DIC test, images were taken at 10-s intervals for the first 50 images, then once past yield, at 40-s intervals.

Figure 6 compares the tensile stress-strain curves, based on extensometer and DIC measurements, from the two tests. The agreement between the stress-strain curves from the different

tests is excellent. The DIC sample failed earlier than the extensometer sample leading to different extensions to failure, but this is not believed to be as a result of the measuring process. The implemented DIC monitoring system and analysis approach therefore captured the average deformation response with high accuracy.

To test the long-term stability of the DIC measurement system, a creep deformation validation test was performed on a plain specimen made from parent AISI Type 316H stainless steel. A load was applied giving a nominal stress of 330 MPa in the gauge section at start of life. The creep test
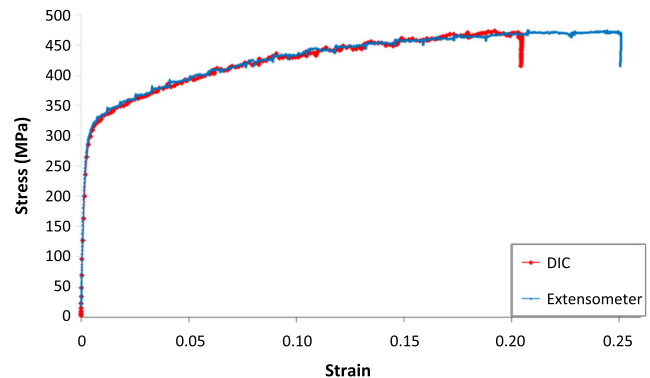

Fig. 6 Tensile stress-strain curves for austenitic stainless steel at 550 °C comparing results of the two separate validation tests, one with the strain measured by an extensometer and the other by DIC

was conducted at a temperature of 550 °C and continued until specimen failure. Images were taken at one-hour intervals and in total 480 images were taken of the specimen during the test. The extension of the gauge section was also simultaneously measured using a high temperature drop down extensometer cradle and a pair of LVDT extensometers, as shown in Fig. 2(b). A shorter (30 mm gauge section) sample than in the later tests was used, enabling the strain in the entire gauge length to be measured using DIC, so that it could be directly compared to the LVDT data.

The resulting displacement vectors calculated by DIC were analysed to obtain the strain evolution in the entire gauge section. Figure 7 compares creep deformation-time curves based on strain measured by a conventional extensometer with curves based on strain measured by DIC monitoring over the gauge length. There is good agreement between the DIC results (orange open circles) and the LVDT values. Although substantial effort was made to reduce the thermal air currents in and outside the furnace, this is still the most likely primary cause of the scatter seen in the results. When images are analysed singly the effect of the thermal currents are clear to see in the displacement data. To reduce this effect, and to aid comparison with the LVDT data, the images were first shift corrected to sub-pixel accuracy and then groups of three images were averaged. These averaged images then underwent the same process route as the single images and the result can be seen as the closed blue circles in Fig. 7. This shows even better agreement with the LVDT data, and that image averaging can be used to reduce the effect of heat haze for DIC.
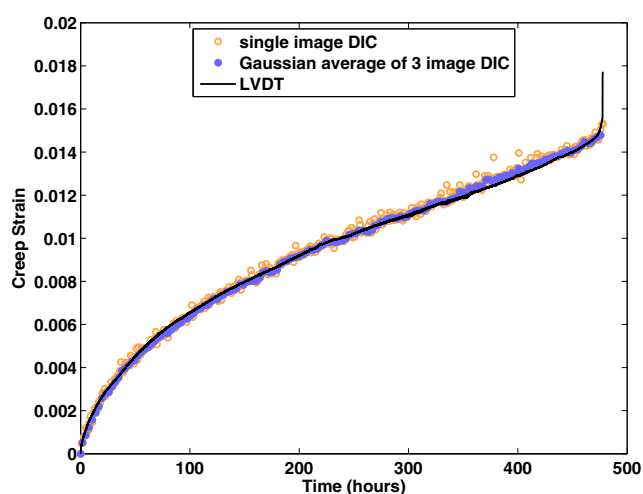

Fig. 7 Creep deformation-time curves for austenitic stainless steel at 550 °C under an applied stress of 350 MPa, comparing results based on strain measured by a conventional extensometer (LVDT) and DIC over the gauge length

Cross-Weld Creep Deformation Measurements

Electro-discharge machining (EDM) was used to extract cross-weld specimens (of the design shown in Fig. 3) from the AISI Type 316H austenitic stainless steel thick section welded plate at two locations (labelled external and internal) as shown in Fig. 1. Creep tests were carried out at 545 °C in a constant load creep frame with the DIC high temperature measurement system described in High Temperature DIC System for Creep Tests section above. A source image, displacement vector and local longitudinal strain maps for the internal sample after 1000 h are shown in Fig. 8. The applied stress, temperature range, local elongation and rupture time for both creep tests are summarised in Table 2. The location of failure for each position is illustrated in Fig. 1. The external creep specimen failed in the parent material, and the internal specimen in the 45° inclined HAZ region. This diagram also marks the failure location of cross-weld tensile tests conducted at room temperature and 545 °C, details of which can be found elsewhere [10, 18].

The arbitrary zero point in all figures is taken as the 90° weld/HAZ interface, with positive values denoting the parent side. Negative position values refer to positions on the weld side. For the external sample all negative values are in the weld, but in the internal sample the 45° weld/HAZ interface is at −8 mm and parent material beyond this point. Examples of the output from the DIC analysis at 1000 h for the internal creep specimen are shown in Fig. 9. There is a noticeable variation in calculated creep strain across the weld line in the internal specimen. This is unsurprising given the differing angles of weld preparation (90° and 45°) producing HAZs of different geometries (see Fig. 1). However, in the cross-weld specimen cut from the external location, only a single weld interface is present at the centre of the specimen and this is perpendicular to the gauge axis. In this configuration a more uniform response across the specimen was observed. The variation in measured creep strain along each cross-weld test specimen as a function of exposure time is illustrated in Fig. 10(a) and (b) for the external and internal creep specimens respectively. In Fig. 11 the in-plane creep shear strain is plotted for the external sample for the weld region only. It is of particular interest to notice a weld bead by weld bead variation in creep strain, with the weld beads being approximately 6.5 mm wide. It appears that the multi-pass weld metal exhibits inhomogeneous creep behaviour, with the centre of each bead showing higher maximum shear strain than the edges of the bead.

The creep deformation across each specimen was highly variable (see Fig. 10), but in each case minimum creep strains accumulated in the HAZ regions (i.e. within about 3 mm of the fusion boundary). Figure 12(a) shows the creep in the parent across the two tests. The external sample failed in the parent material and so the creep curve at that point has been

Fig. 8 DIC analysis of strain in the gauge section in the internal specimen from the stainless steel weldment at a creep life of 1000 h. On the left, the original image with pseudo colours, in the centre is the calculated displacement map and on the right is longitudinal local strain map. The 45° HAZ interface is at position 2485 pixels and the 90° HAZ interface is at 1678 pixels
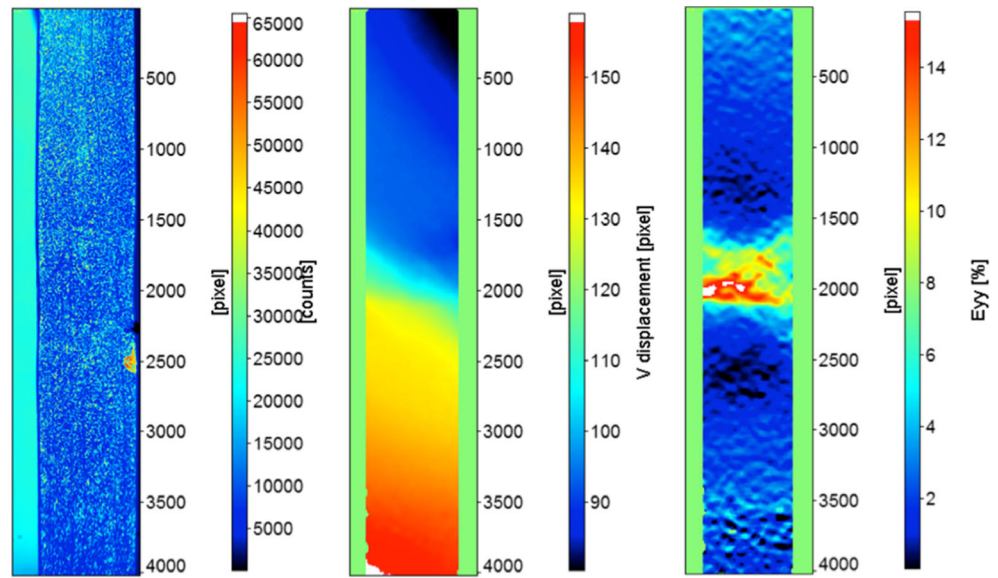
plotted. In contrast, the parent material on both sides of the weld exhibited consistent behaviour along the analysed region. To reduce the scatter in the data for these low strain values, which otherwise would have a much lower signal to noise ratio, the average strain across a region of 10 mm has been plotted. Both regions of parent material in the internal sample show a very similar creep response. The external sample parent data is also quite similar, but as the test lasts longer it eventually fails in this region.

The root position (internal) test specimen failed at a significantly shorter life than the external position (Table 2). Rupture occurred in the HAZ just to the left of the weld root (x = −8 mm) where the final logged local axial creep strain (averaged across thickness) was 0.02. After this point a macroscopically visible crack formed. The opening of this crack produces the spike up to 0.08 in Fig. 9 and 10(b) in the same position, but as this strain was calculated across a visible crack the value does not represent the strain in the material at this point, which was still 0.02. The creep deformation curves for the HAZ to either side of the root weld in the internal specimen are very similar up to 600 h (Fig. 12(b)), but then the creep rate for the 45° inclined HAZ significantly increases. This increase in HAZ creep deformation rate is probably

caused by the large creep strains being accumulated in the adjacent weld metal, (see Fig. 10b), and the fact that the fusion boundary on this side was not normal to the loading direction. The rupture occurred entirely in the HAZ material with the fracture face lying parallel to the fusion boundary.

Figure 12(c) shows the creep data for the weld material. In the external sample the creep strain rate was relatively constant along the weldment and so the data has again been averaged along a 10 mm length. The internal sample has a peak strain rate in the centre of the weld section (Fig. 10(b)) and so this single point has been used to plot the creep strain for the weld in this sample. The peak strain and strain rate for the weld are much higher in the internal sample than the external. However, the regions do have very different local constraint and thermal histories due to the welding process.

Discussion

The conditions that have to be met to complete a successful creep test with in-situ deformation monitoring using DIC are more stringent than those for a conventional creep rupture test. A uniform temperature along the test specimen gauge length

Table 2 Applied stress, temperature, duration and elongation of each creep test for AISI 316H cross-weld specimens

Position	Top	Bottom	Validation
Applied stress (MPa)	315	313	330
Temperature (°C)	545 ± 1	545 ± 1	550 ± 1
Failure location	Parent (x = 18 mm)	HAZ (x = −8 mm)	Shoulder interface
Local ductility (%)	21	2.1	1.5
Test duration (h)	2187	1339	480

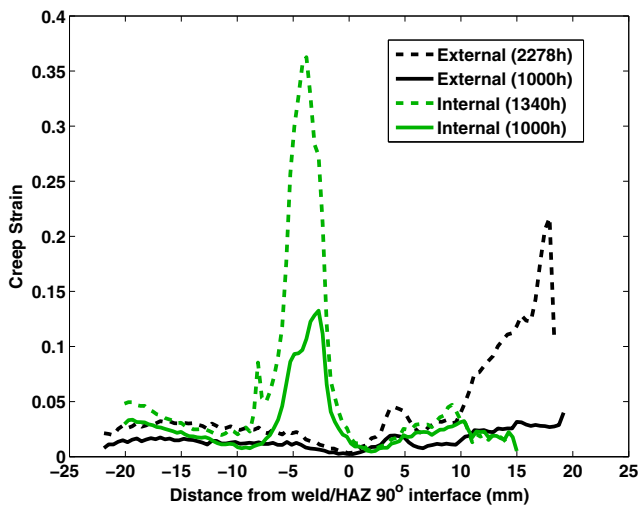Note: the fusion boundary is at x = 0 mm

Fig. 9 Average strain across the width along both external and internal samples at 1000 h and at failure, with an applied stress of 315 MPa at 545 °C

Fig. 11 Creep strain distribution across the weld region of the external sample after 2250 h showing inhomogeneous behaviour due to weld beads (size ~6.5 mm)

must be maintained as for a standard test [27], but this requirement could be compromised by the introduction of the porthole in the furnace. However this has been shown to be a small effect for the present system, probably owing to the relatively small dimensions of the porthole and because a window was fitted with an effective seal. It is worth noting that local variations in creep deformation response along the test specimen gauge length owing to differences in temperature will be measured by the DIC monitoring system. This effect is averaged out by conventional extensometry, and while it can be averaged out when using DIC, the advantage of resolving local behaviour would be removed also. Therefore it is particularly important to create a uniform temperature along the gauge length in DIC monitored tests, to maintain the validity of the spatially resolved data. Like conventional creep testing, it is also important to control the ambient temperature in the creep
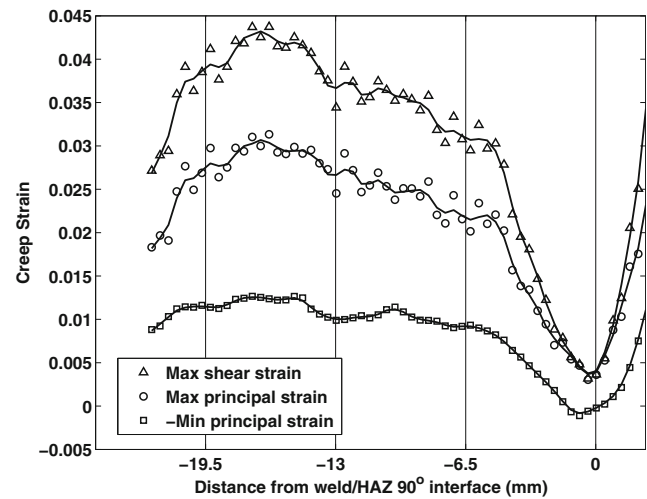
laboratory [27], as variations in temperature outside of the furnace affect the test specimen temperature, creep response and imaging conditions. This is particularly important due to the large thermal mass of the pull-rod and grip assembly, in comparison to the sample, acting as a heat sink. Approximately half of the length of the pull-rods extends from the furnace, with this region being exposed and affected by any change in laboratory ambient conditions.

The requirement for the viewed gauge length of the test specimen to be flat can introduce stress concentrations, where the cross-section changes to provide a threaded fixing, and therefore the geometry must be carefully designed [28]. The gauge length and cross-sectional dimensions of the specimen are an important variable when testing cross-weld specimens where the creep response of the material is sensitive to constraint, for example the fine grain HAZ of high Cr martensitic
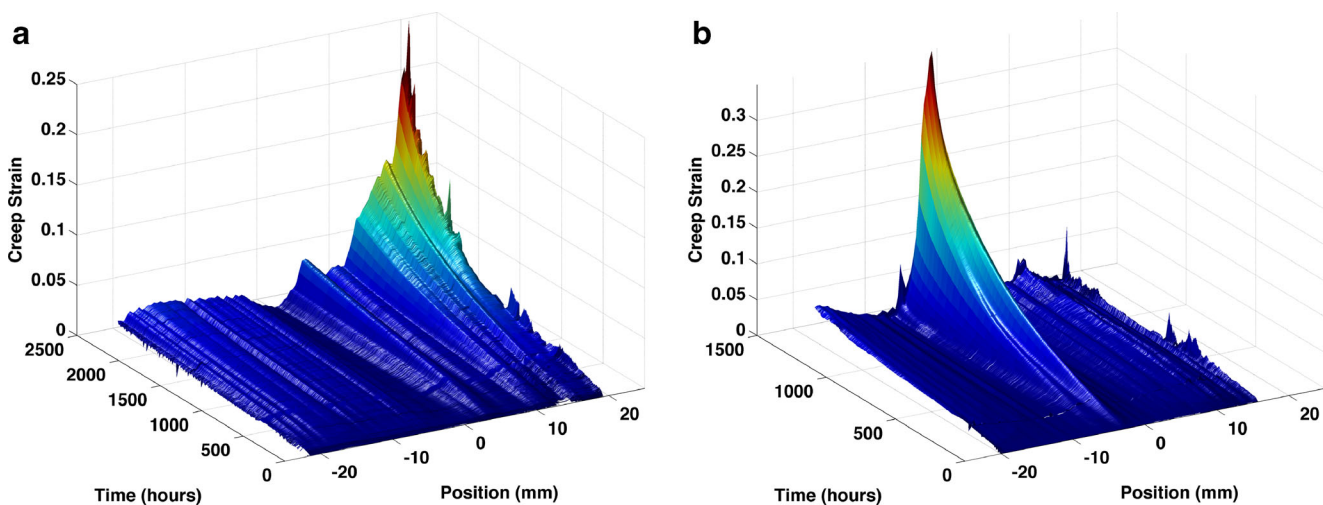

Fig. 10 3D surface plots showing the variation in measured creep strain along the gauge lengths relative to the weld/HAZ 90° interface of (**a**) the external, (**b**) the internal stainless steel cross-weld test specimens as a function of test duration for an applied stress of 315 MPa at 545 °C
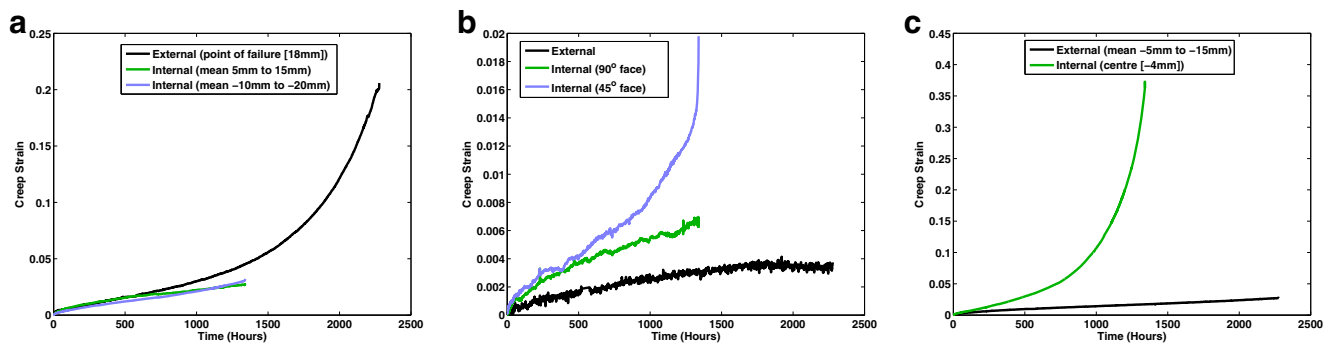
Fig. 12 Comparisons of (**a**) parent, (**b**) HAZ and (**c**) weld metal creep deformation curves from external and internal cross-weld test specimens for an applied stress of 315 MPa at 545 °C

steel welds where Type IV cracking develops in the overtempered, intercritical or refined HAZ [29]. Sharply varying tensile and creep deformation properties along cross-weld test specimens can also affect the local distribution of strain measured by DIC [30].

Wire electro-discharge machining (EDM) is often used to produce flat creep test specimens. For DIC this method also has the advantage of producing a speckle finish on the cut surface. Specimens made in this way from stainless steel may not need application of any paint, provided sufficient image contrast is obtained from this "natural" speckle. In tests where oxidation effects are minimal (e.g. for high temperature tensile tests), this surface preparation method may be particularly suitable. In general, a paint system must be applied to the surface of the gauge length, if it is to be monitored by DIC, in order to produce a suitable speckle finish. These speckles must not significantly degrade during the creep test, which may last for several thousands of hours. The silica ceramic-based paint (VHT FlameProof™) system has been successfully applied by the authors to austenitic stainless steel creep test specimens tested at temperatures up to 675 °C for at least 3000 h. The paint was also stable enough over the test period that all the correlations were performed using the first image as a reference. In combination with the separate validation test, where long-term high-temperature DIC is compared with conventional extensometry, this gives confidence in the absolute values of results.

Stable lighting conditions are required throughout the creep test. Consistent illumination of the test specimen is required for each image taken, in order to maximise the robustness of the DIC analysis, Ideally ambient lighting must also be controlled, for example by locating the test rig in a darkened room or shielding the light path. This is required, not only to reduce any changes in lighting intensity on the speckle pattern, but also to reduce the likelihood of reflections in the furnace window being captured by the camera.

The imaging camera must be rigidly held relative to the test specimen load train frame so that the same field of view can be maintained for several thousands of hours. When using DSLRs for DIC, effort must be made in the set up to reduce or remove the effect of vibration caused by the mirror and shutter. Ideally the DIC monitored creep test system needs to be situated in a vibration free laboratory and isolated from the risk of human disturbance. Thermal haze is another issue that must be controlled [30], for example by fitting and sealing a closely fitting glass window to the access porthole (as described earlier). Once the haze is reduced to a low-level, image averaging can be used to stabilise the speckle pattern before the DIC analysis is performed.

The type of glass used for the window must be of optical quality and not degrade with time when exposed to high temperatures (optical quartz or preferably optical sapphire windows are recommended by the authors). The window should also be as thin as possible so that chromatic aberration at the extremes of the image, caused by varying optical path length through the window, is minimised. This is of particular concern if a colour camera is used, as a monochromatic light source or bandpass filter cannot be used to negate this without losing image quality.

It is desirable to use a control system to vary the frequency of image acquisition with changes in the instantaneous strain during the creep test. For example an increased acquisition rate is needed during primary and tertiary creep, whereas the rate can be reduced during secondary creep. Creep tests can generate very large volumes of image data, and systems have to be developed to handle this. If the sample does not fill the image, then the unused portion of the image can be cropped to reduce the storage requirement without losing useful data. In addition, interactive analysis of acquired images should be conducted in order to check the quality of the data and progress of the creep test.

When performing the DIC analysis to provide the raw data for the creep curve extraction process, it was found that increasing the density of vectors reduced the scatter in the creep curves. However, the improvement reaches a plateau as the step size reduces to that of the speckle size. The step size of 7 pixels used here was found to be a good compromise between accuracy and volume of data. Averaging the strain across 100

regions produced good quality creep curves. Performing outlier removal at this step, where the performance of a small region is considered, rather than filtering the data using a more local approach, was found to give more robust and accurate data. When using a region overlap of 75%, it was found that for these tests using the Nikon D300, 100 equal regions provided a balance between accuracy and resolution. This figure is dependent on the noise of individual displacement vectors and the resolution of the camera, and so should be considered separately for each set of tests.

Using a surface strain measurement technique such as DIC to measure strain in a complex test specimen, such as these cross-weld samples, should be approached with caution. The local constraint caused by the locally varying (elastic, plastic and creep) properties will lead to a tri-axial stress state to some degree, and whether this has a significant effect on the eventual results should be assessed on a case by case basis [31]. For example, in Fig. 9 the minimum strain along the specimen

immediately before failure for the external sample is at 0 mm, directly on the fusion boundary, in a region where there are no large strain gradients. For the internal sample, the minimum strain before failure is located at 2 mm. However, in contrast to the external sample, the internal sample has a very high strain gradient (0.30 to 0.01 strain across 5 mm) suggesting that the appearance of a minimum strain point away from the fusion boundary is most likely due to a material properties discontinuity effect.

When considering the results around the 45° HAZ region in the internal sample, care must be taken to account for the variation in mechanical properties through the thickness. DIC can only measure the strain on the surface, and so the 45° HAZ will have a direct effect on the material behaviour over a larger region than the perpendicular HAZ region (Fig. 13), creating ambiguity if material properties are being measured. The internal sample was tested in the same configuration as face B in Fig. 13, so the fusion zone will have had a

Fig. 13 Weld geometry of internal cross-weld sample, showing the projection of the 45° angled HAZ on the surface used for DIC
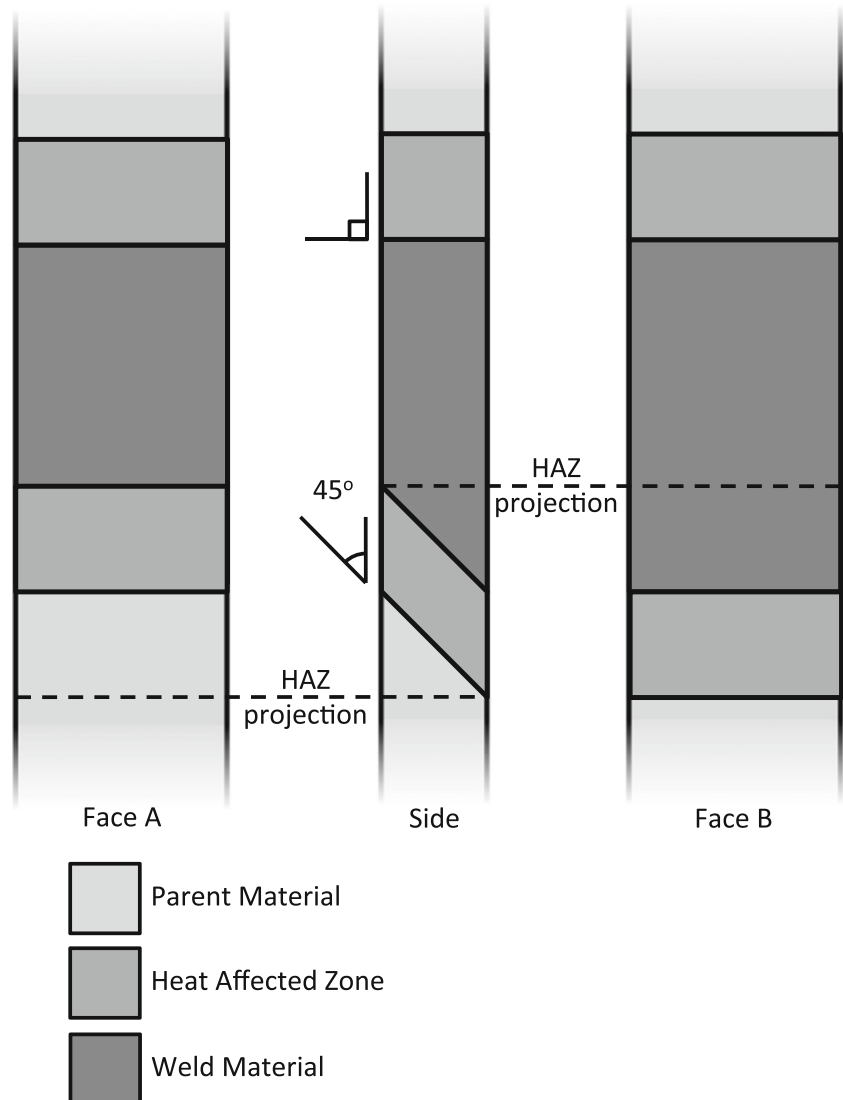
disproportionate effect on the neighbouring HAZ region measurements. Without interfacing the DIC data with a model of the geometry and employing an inverse method to solve for the material properties [32, 33], knowledge of these phenomena can at least inform interpretation of the results. This 45° HAZ boundary may also cause a small amount of bending out-of-plane during the test. Using 2D DIC it is not possible to distinguish this bending from material phenomena, but no bending was detectable after failure. If bending did occur, due to the long load chain and universal joints at either end, the neutral axis would deviate little. The large working distance of the camera also helps to minimise the sensitivity of 2D DIC to out-of-plane displacement.

The cross-weld creep deformation results presented in Cross-weld Creep Deformation Measurements Section demonstrate the rich measurement data that can be collected from DIC monitored creep tests. One hundred creep curves characterising the local creep deformation response were measured simultaneously. Each of these curves can be analysed to determine the creep strain rate as a function of time and minimum creep strain rate. The transverse strain can also be analysed and the net section reduction of area inferred (assuming isotropic Poisson's strain in the thickness direction), and thereby the true stress averaged over any gauge cross-section determined. These data can be used to help understand the complex behaviour of welds as illustrated for the thick section multi-pass stainless steel weld. The next step is to use inverse methods, for example [6], to analyse the data and develop new constitutive models describing the deformation behaviour of parent, HAZ and weld materials.

The high temperature DIC monitoring system described in this paper has much untapped potential. The temperature range can be readily extended to 1000 °C. Creep deformation under varying stress levels could be examined in a single sample by using a tapered gauge length. Similarly, a temperature gradient could be applied to a parallel-sided sample with the temperature variation measured using a thermal camera. A DIC system could be developed for strain controlled creep-fatigue and creep crack growth tests, or to examine the response of large, welded test components. For materials susceptible to oxidation, more sophisticated systems could be designed for a high temperature environmental or vacuum chamber. Where non-flat test components are of interest (e.g. notched bar specimens) or where out of plane deformation is important, then in principle, specimens can be monitored in 3D using two cameras at high temperatures.

Conclusions

In this study, it has been demonstrated that a DIC monitoring technique can provide measurements of local variations of elastic, plastic and creep strain in inhomogeneous materials at elevated temperatures. The DIC measurements have been validated against extensometer measurements during high temperature tensile and creep tests at 545 °C. The technique has been successfully used to acquire full field strain data in stainless steel cross-weld samples at 545 °C as a function of time, during creep tests enduring a few months.

The creep tests on cross-weld specimens machined from an AISI 316H austenitic stainless steel weldment showed that the creep performance of the multi-pass weldment is complex, depending on the local creep deformation properties and ductility. Low magnitude creep strains (under ≈0.02) accumulated in HAZ regions (within about 3 mm of the fusion boundary) for both test specimens.

The ability to measure spatially resolved creep strains with high accuracy opens up the possibility of a new paradigm for long term material testing. Collecting 100 creep curves in this way may not directly replace 100 uniaxial creep tests, but to obtain the resolution of material variation shown here would require very small samples, and this presents its own challenges for creep testing. Also, the spatial relationships of the creep response between different regions of the weld are also implicitly gathered at the same applied stress level and test temperature. This information could be accessed by fitting a function to the creep response surfaces (e.g. Fig. 10) to produce a continuous definition of creep behaviour for a weld.

References

1. Francis JA, Mazur W, Bhadeshia HKDH (2006) Review type IV cracking in ferritic power plant steels. Mater Sci Technol 22:1387–1395

2. Energy Nuclear Generation Ltd EDF (2012) R5 assessment procedure for the high temperature response of structures. Revision 1

3. Kartal M, Molak R, Turski M et al (2007) Determination of weld metal mechanical properties Utilising novel tensile testing methods. Appl Mech Mater 7–8:127–132. doi:10.4028/www.scientific.net/AMM.7-8.127

4. Boyce BL, Reu PL, Robino CV (2006) The constitutive behavior of laser welds in 304 L stainless steel determined by digital image correlation. Metall Mater Trans A 37:2481–2492. doi:10.1016/j.msea.2005.09.032

5. Hatamleh O (2008) Effects of peening on mechanical properties in friction stir welded 2195 aluminum alloy joints. Mater Sci Eng A 492:168–176. doi:10.1016/j.msea.2008.03.017

6. Avril S, Pierron F, Sutton MA, Yan J (2008) Identification of elasto-visco-plastic parameters and characterization of Lüders behavior using digital image correlation and the virtual fields method. Mech Mater 40:729–742. doi:10.1016/j.mechmat.2008.03.007

7. Molak RM, Paradowski K, Brynk T et al (2008) Measurement of mechanical properties in a 316 L stainless steel weldedjoint. Int J Press Vessel Pip 86:43–47. doi:10.1016/j.ijpvp.2008.11.002

8. Acar M, Gungor S, Bouchard P, Fitzpatrick ME (2010) Effect of prior cold work on the mechanical properties of weldments. Proc. 2010 SEM Annu. Conf. Expo. Exp. Appl. Mech. 7–10 Jun 2010, Indianapolis, Indiana, USA

9. Sakanashi Y, Gungor S, Bouchard PJ (2011) Measurement of Creep Deformation in Stainless Steel Welded Joints. In: Proc. SEM Annu. Conf. June 13–16, 2011 Mohegan Sun, Uncasville, Connect. USA. pp 415–422

10. Sakanashi Y, Gungor S, Bouchard PJ (2012) Creep Deformation Measurement of 316H Stainless Steel Multi-passs Welded Joints using Digital Image Correlation. 4th Int. Conf. Integr. High Temp. Welds/Creep Conf. Proceeding 2012, London UK

11. LaVision (2014) StrainMaster 8.2. LaVision GmbH, Goettingen

12. Sutton MA, Schreier H, Orteu JJ (2009) Image correlation for shape, motion and deformation measurements: basic concepts, theory and applications. Springer-Verlag U.S., Berlin

13. Lucas BD, Kanade T (1981) An iterative image registration technique with an application in stereo vision. In: Seventh Int. Jt. Conf. Artif. Intell. pp 674–679

14. Bouguet J-Y (2000) Pyramidal implementation of the Lucas Kanade feature tracker description of the algorithm. Intel Corp Microprocess Res Labs. doi:10.1016/j.tim.2005.08.009

15. Fleet DJ, Weiss Y (2005) Optical Flow Estimation. In: Handb. Math. Model. Comput. Vision. Springer, pp 239–258

16. Lyons JS, Liu J, Sutton MA (1996) High-temperature deformation measurements using digital-image correlation. Exp Mech 36:64–70

17. Forsey A, Gungor S (2016) Demosaicing images from colour cameras for digital image correlation. Opt Lasers Eng 86:20–28

18. Sakanashi Y (2013) Measurement of Creep Deformation in Weldments. PhD Thesis. The Open University

19. Grant B, Withers PJ, Preuss M, Stone H (2009) High-temperature strain field measurement using digital image correlation. J Strain Anal 44:263–271. doi:10.1243/03093247JSA478

20. Nikon Japan (2014) Nikon D810 User Manual

21. Sutton MA, SR MN, Helm J, Yuh C (2000) Advances in two-dimensional and three-dimensional computer vision. Top Appl Phys 1:323–372

22. Reu P (2014) All about speckles: aliasing. Exp Tech 38:1–3

23. Reu P (2015) All about speckles: speckle density. Exp Tech 39:1–2

24. Bayer B (1975) Colour imaging array

25. Mathworks Inc (2013) MATLAB 2013a

26. Clocksin WF, Chivers KF, Torr PHS et al (2002) Inspection of surface strain in materials using dense displacement fields. Proc Int Conf New Challenges Mesomech Aaalborg Univ Denmark 2:467–475

27. ASTM (2009) ASTM E-139 Standard Test Method for Conducting Creep, Creep-Rupture and Stress-Ruptured Test of Metallic Material

28. Mayr P, Mendez-Martin F, Albu M, Cerjak H-H (2009) Correlation of Creep Strength and Microstructural Evolution of a Boron Alloyed 9Cr3W3CoVNb Steel in As-Received and Welded Condition. In: Creep Fract. High Temp. Components–ECCC, Zurich, Switz. pp 1029–1037

29. Abson DJ, Rotwell JS (2013) Review of type IV cracking of weldments in 9-12% Cr creep strength enhanced ferritic steels. Int Mater Rev 58

30. Doosan Babcock Energy (2009) Production of stainless steel butt weld on ex-service headers

31. Acar MO, Gungor S (2015) Experimental and numerical study of strength mismatch in cross-weld tensile testing. J Strain Anal Eng Des 50:349–365. doi:10.1177/0309324715593699

32. Pannier Y, Avril S, Rotinat R, Pierron F (2006) Identification of elasto-plastic constitutive parameters from statically undetermined tests using the virtual fields method. Exp Mech 46:735–755. doi:10.1007/s11340-006-9822-x

33. Grédiac M, Avril S, Pierron F, Toussaint E (2006) The virtual fields method for extracting constitutive parameters from full-field measurements: a review. Strain 42:233–253. doi:10.1111/j.1475-1305.2006.00283.x